

Return Flow Generating Point on a Hillslope Layered with Traffic Pan

DEB Sanjit Kumar, MIYAZAKI Tsuyoshi, MIZOGUCHI Masaru and SEKI Katsutoshi*

*Graduate School of Agricultural and Life Sciences, the University of Tokyo,
1-1-1 Yayoi, Bunkyo-ku, Tokyo 113-8657, JAPAN.

Abstract

Two-dimensional soil water movement under the rainfall infiltration has been demonstrated using the model slope layered with traffic pan. The experimental runs of the 8° and 12° model slopes under the prolonged steady rainfalls of 80, 100, 125, and 150 mm h⁻¹ suggest the development of the perched saturated zone above the underlying traffic pan as well as the downslope subsurface flow ensues. Confining attention to flow in evolved saturated zone at steady state, the concept for predicting the evolution of the slope surface saturation is introduced as Return Flow Generating Point (RFGP), the location of the intersection of the perched water table (PWT) and the slope surface attributed to the return of infiltrated rainwater. RFGPs observed from the eight experimental runs are presented, discussed, and generalized to imply RFGP on a long uniform hillslope layered with existent traffic pan.

Key words : Unsaturated soils, Traffic pan, Model slope, Return Flow Generating Point

1. INTRODUCTION

Tracked and wheeled vehicles used during the extensive tillage operations in Tsumagoi (Gunma Prefecture, Japan) hillslope agricultural fields have eventually resulted traffic pan in unsaturated soils. Traffic pan in such fields has been characterized by high bulk density and very low saturated hydraulic conductivity. Since densely-packed traffic pan may create conditions that restrict water percolation during the rainfall episodes, the hydraulic conductivity contrast between the top and traffic pan layers may lead to the development of the perched saturated zone, and the downslope saturated flow ensues above the underlying traffic pan. In addition, the existence of traffic pan may accelerate soil erosion, and may change landscape hydrology as well. The most baffling observation of Tsumagoi hillslope fields is that gullies and rills are developed mostly by extending their upper end uphill. This upward advance of erosion channels is often caused by undermining, which seems to be due to water coming out of the soil and not pouring over it. Such undermining of erosion is obviously followed by return flow and then by runoff (Zaslavsky and Sinai, 1981a).

During the past several decades, water movement to and through the hillslope riparian zones has been stressed repeatedly in numerous field studies. A comprehensive summary of these studies concerned with saturation-excess runoff mechanisms in the soil-bedrock interfaces is given by Anderson and Burt (1990). Despite decades of increasingly intensive focuses on hillslope runoff mechanisms, field studies

clearly demonstrated that subsurface flows dictated the occurrence of hillslope variable saturated areas, which in turn caused return flow and influenced the storm runoff behaviors in the hillslope-riparian interactions (e.g., Weyman, 1973; Dunne et al., 1975; Whipkey and Kirkby, 1978).

Since hillslope hydrologic interactions between surface and subsurface waters occur by lateral subsurface flow through the unsaturated soil and by infiltration into or return flow from the saturated zones, the potential for the slope saturation is therefore a position dependent attribute in the slope topography. The importance of hillslope topographic index in investigating the occurrence of the saturated source areas formation has been recognized as a consequence of several experimental studies (e.g., O'Loughlin, 1981; Aryal et al., 2002). O'Loughlin (1981) derived criteria for the existence of the saturated areas on draining hillslopes in the natural catchments. Criteria were given in terms of soil transmissivity (the hydraulic conductivity times the depth of saturation) above the underlying bedrock, hillslope geometry, and its wetness state located by the groundwater intercept and characterized by the base flow discharge from the catchment. The effects of soil transmissivity, hillslope geometry, and drainage flux density were lumped into a dimensionless parameter whose value determined the location of seepage boundaries on hillslopes of the specified geometry. Aryal et al. (2002) investigated the catchment landscape saturation using the similarity parameters approach derived from the topographic, soil, and climate attributes.

Three parameters, i.e., input index that provided the aggregated effects of hillslope attributes (scale and soil) and drainage in causing the saturation, the slope convergence ratio (the ratio of the ridge length to the outlet length), and profile factor (the degree of concavity or convexity of the profile) defined the extent of hillslope saturation. From these three parameters, a single dimensionless parameter has been derived to describe the occurrence of saturation in planar, concave, and convex profile hillslope shapes.

Although much attention has paid to the occurrence of hillslope saturated source areas in the field studies, there might have not been any reported observation especially for the saturated area formation in hillslope layered with traffic pan. The unsaturated soils with existent traffic pan in Tsumagoi hillslope fields may be explicit controls of the local phenomena and attributes. There remains room for substantial research to investigate the evolution and extent of specific hillslope saturation under the controlled laboratory conditions. Therefore, the purpose of this paper is two-fold. The study primarily presents the results obtained from the laboratory model of hillslope two-dimensional soil water movement in unsaturated soils layered with traffic pan under the steady rainfalls to observe the effect of such pan. Secondly, the study approaches the possibility of confining subsequent attention mainly to flow in the evolved saturated zones to observe Return Flow Generating Point (hereafter, referred to as RFGP), which is defined as location of the intersection of the perched water table (hereafter PWT) and the slope topography attributed to the return of infiltrated rainwater.

2. CHARACTERIZATION OF TRAFFIC PAN IN HILLSLOPE FIELD

Agricultural hillslope fields were located near the Alpine Crops Research Center, Tsumagoi. A hillslope plot ($100\text{ m} \times 40\text{ m}$) having an average, uniform slope of 8° was chosen for characterizing the presence of traffic pan. Surface elevations were surveyed using the dumpy level instruments. Two sampling sites were established at the upslope and downslope portions in order to determine bulk density, the saturated hydraulic conductivity, soil resistance, and particle size distribution in the soil profiles.

Typical stratification of volcanic ash soil (Andisol) profiles in the sampling pits comes as follow: 0 to 30 cm – plow layers; 30 to 40 cm – successive layers; 40 to 60 cm – natural hard brown layers; and depth > 60 cm – gravel layers. Bulk density and the saturated hydraulic conductivity were determined using standard 5 cm diameter, and 5 cm depth soil core samplers. These core samplers were taken in triplicate at 5 cm depth increments from 0 to 50 cm depth, and the soil was excavated in 5 cm increments assuring a level surface each time.

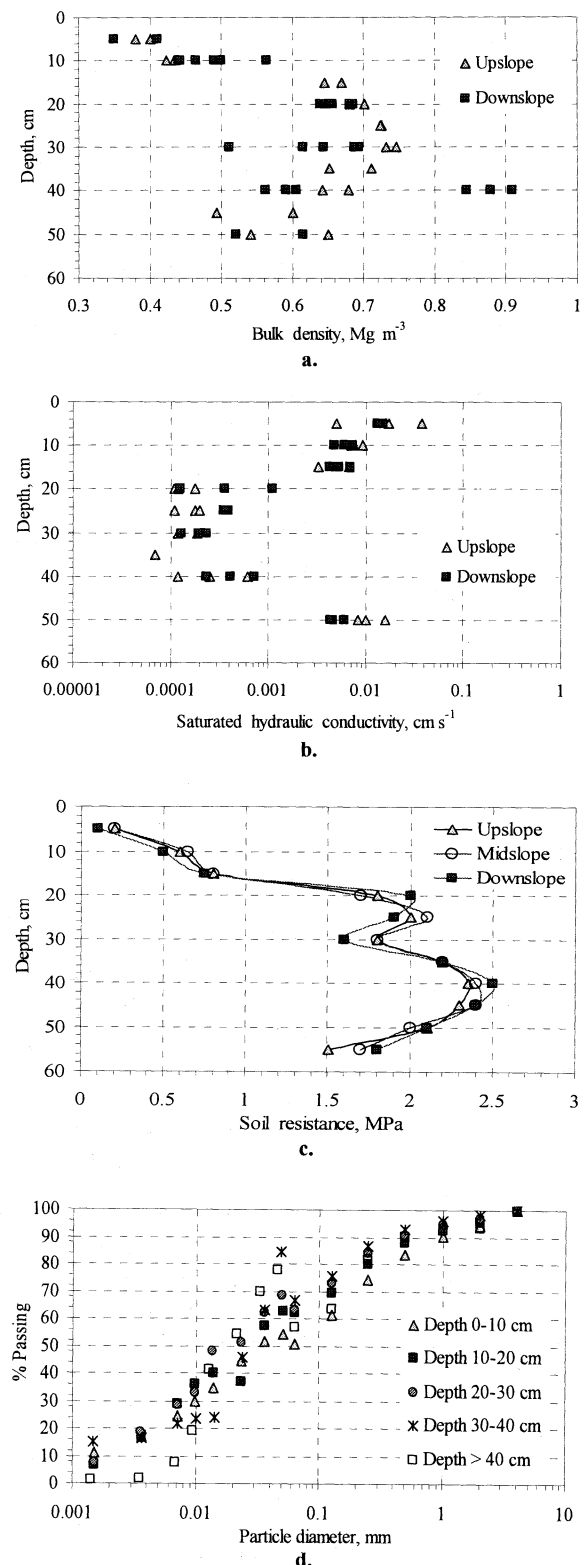


Fig.1 Physical properties of volcanic ash soil (Andisol) versus the soil depth in Tsumagoi (Gunma Prefecture, Japan) hillslope field layered with traffic pan at 20 cm depth:
 (a) bulk density; (b) saturated hydraulic conductivity;
 (c) Soil resistance; and (d) particle size distribution.

Bulk density and the saturated hydraulic conductivity values of these undisturbed soil samples were determined using the core and falling head methods, respectively. Volumetric water content was determined from gravimetric water content. Soil resistance was measured within a $10\text{ m} \times 10\text{ m}$ sub-plot at the midslope using a cone penetrometer. The sub-plot was discretized into $1\text{ m} \times 1\text{ m}$ grids, and soil resistance was measured at the nodes of each square grid along and across the sub-plot. Particle size analysis was applied using the sieving and pipette methods on soil samples taken from five different depths of 0-10, 10-20, 20-30, 30-40, and depth > 40 cm. Acute increments in bulk density (**Fig.1a**) at 20 cm depth confirm the presence of traffic pan. The saturated hydraulic conductivity (**Fig.1b**) tends to decrease with the increasing depths of 0-40 cm, especially with the sharpest decrease occurring at traffic pan depth 20 cm. Traffic pan depth was also inferred from soil resistance values along the slope of the sub-plot. Average soil resistance values (**Fig.1c**) across the upslope, midslope, and downslope transect of the sub-plot suggest the presence of dense traffic pan layer at a depth of 20 cm. However, particle size analysis (**Fig.1d**) does not reveal any significant changes in fraction distributions versus the soil depth.

3. THEORETICAL CONSIDERATIONS

3. 1 General Description of the Flow Region

To derive the two dimensional flow region of interest for Tsumagoi hillslope, the vertical cross-section of a sloping rectangular region ABCD illustrated in **Fig.2** is considered. The top layer of depth D_1 is underlain by traffic pan layer of depth D_2 , and the saturated hydraulic conductivity of the top layer (K_{s1}) is much greater than that of the subjacent pan layer (K_{s2}). The x axis is positive in the downslope direction with origin at the hillslope crest, and the z axis is positive downward. Slope profile and soil depth are uniform for the entire length of the slope.

Boundary AB allows rainfall infiltration. CD is no flux boundary because of the existence of traffic pan and the subjacent natural hard brown layers in Tsumagoi hillslope soil profiles. Since conductivity contrasts across this boundary are large enough it is justified in taking the bottom boundary CD as impermeable, and disregarding the very negligible contributions to the flow system that may occur below it. DA is no flux boundary since it corresponds to the upslope divide of the hillslope, i.e., it separates the region of flow from the adjacent hillslope at the upslope. BC is no flux boundary for the two reasons based on the observations of Tsumagoi hillslopes: (i) there is no incised stream channel at the bottom of the hillslope, and (ii) the hillslope opposing the hillslope is identical in character so that BC becomes a line of symmetry, i.e., boundary BC is in the plane separating

the fields of flow of the two hillslope sections at the bottom of the hillslope. Such a symmetry condition of flow decrees that there is no flux across this plane. These features of Tsumagoi hillslopes considered in this study belong to the upper portions of the first-order basin class (Huggett, 1975). It is therefore assumed that runoff removes from this flow region and drains sporadically at the bottom of the hillslope.

3. 2 Conceptualization of the Flow

Rainwater infiltrates into the slope surface and percolates downwards, raising soil water content as it goes. When the percolating rainwater reaches the interface between the highly permeable top and very low permeable traffic pan layers, the interface starts to become saturated. Within traffic pan layer, a wetting front may slowly percolate downwards. Meanwhile, a saturated layer in the form of triangular wedge tends to develop at the downslope above traffic pan layer (**Fig.2**). Rainwater percolating to this saturated wedge rises up the saturated zone directly, acting effectively as the PWT within the soil above traffic pan layer. At any moment, however, discharge from the downslope is related to this saturated wedge within which water moves according to Darcy's law (Weyman, 1973; Whipkey and Kirkby, 1978; Anderson and Burt, 1990). During the long wet period, discharge tends towards a steady state. Saturated layer may then build up to the slope surface, producing surface seepage as return flow, and also preventing the entry of further rainfall onto the saturated area, which runs off directly as saturation overland flow. The potential for such slope saturation is therefore an attribute related to the breakout location of the PWT in the slope surface as RFGP (**Fig.2**).

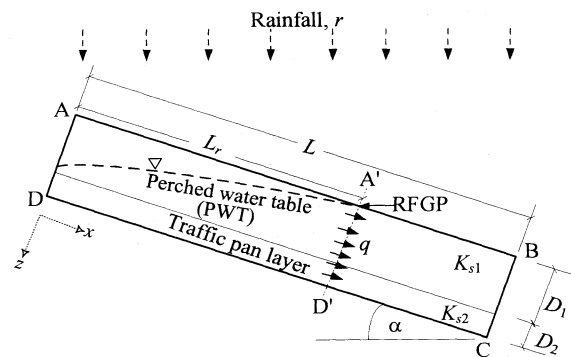


Fig.2 Definition sketch of Return Flow Generating Point (RFGP).

3. 3 Descriptive Equations for RFGP

With reference to **Fig.2**, the intersection of the PWT must coincide with RFGP along the slope. The downslope subsurface flux ensues through this saturated zone is equal to the influx of rainfall above that RFGP. Mass balance at RFGP cross-section (A'D') under steady state can then be expressed mathematically as,

$$rL_r \cos \alpha = qA \quad (1)$$

where r is the steady rainfall flux; L_r is RFGP from the upslope; q is flux at RFGP cross-section; and A is the saturated depth at RFGP section, which represents the soil depth D_1+D_2 . This mass balance is based on the assumption of no flux at the bottom CD.

The saturated zone is fed by water moving out of the unsaturated soils during the prolonged rainfall. Assuming that soil is isotropic, flux q at any depth of unsaturated soils, governed by Darcy's law, is decomposed into q_x and q_z (Miyazaki, 1993),

$$q_x = -K \left(\frac{\partial \psi_m}{\partial x} - \sin \alpha \right) \quad (2)$$

$$q_z = -K \left(\frac{\partial \psi_m}{\partial z} - \cos \alpha \right) \quad (3)$$

$$q = \sqrt{q_x^2 + q_z^2} \quad (4)$$

where q_x the flux component in the direction of the x axis; q_z is the component in the direction of the z axis; K is the unsaturated hydraulic conductivity, which is a function of matric head Ψ_m of the soil water; and α is the slope angle. The K is described by combining the van Genuchten's soil water retention model with the pore-size distribution model of Mualem (van Genuchten et al., 1991),

$$S_e(\psi_m) = \frac{\theta(\psi_m) - \theta_r}{\theta_s - \theta_r} = \left[1 + |\alpha_v \psi_m|^{n/m} \right]^{-m} \quad (5)$$

$$K(\theta) = K_s S_e^{0.5} \left[1 - \left(1 - S_e^{1/m} \right)^m \right]^2 \quad (6)$$

where S_e is the effective saturation; θ_r and θ_s denote the residual and saturated water contents, respectively; K_s is the saturated hydraulic conductivity; and α_v , n , and m ($=1-1/n$) are the model fitting parameters. The Eq. (5) is fitted to the observed soil water retention curves using a nonlinear least-squares optimization approach that minimizes the sum of squared deviations between the observed and the fitted water contents. Of course, for nonnegative Ψ_m , $S_e = 1$, that is, the medium is saturated.

At steady state, it is apparent that lateral subsurface flow is dominated by the inclination of the PWT throughout the downslope saturated zone. However, most of the flow may occur in the highly permeable top layer. The total flow, integrated over the whole saturated depth at RFGP section, must be lateral (Zaslavsky and Sinai, 1981b; Wallach and Zaslavsky, 1991). Assuming that the PWT is always almost parallel with the slope bed so that the hydraulic gradient is equal to the slope surface at RFGP, steady lateral subsurface flow passing through RFGP section is given by,

$$q_x = K_s \sin \alpha \quad (7)$$

Hence, on a given uniform hillslope, RFGP at steady state can be predicted from the Eq. (1),

$$L_r = \frac{q_x A}{r \cos \alpha} \quad (8)$$

Substituting the Eq. (7) into the Eq. (8) yields,

$$L_r = \frac{AK_s \tan \alpha}{r} \quad (9)$$

4. LABORATORY MODEL

4. 1 Materials

Volcanic ash soil collected from Tsumagoi hillslope plot was used for the model slope experiments. Soil physical properties are presented in Fig.1a, Fig.1b, Fig.1c, and Fig.1d. Average values of the saturated hydraulic conductivities and bulk densities for the top soils were 0.014 cm s^{-1} and 0.4 Mg m^{-3} , respectively. These values for traffic pan were $0.00011 \text{ cm s}^{-1}$ and 0.68 Mg m^{-3} , respectively. Soil water retention behaviors determined using the soil column method for the soils are shown in Fig.3.

4. 2 Laboratory Setup

The laboratory model system, illustrated in Fig.4, is composed of a rectangular soil packing Plexiglas box, a slope adjustable support, a rainfall simulator, soil water pressure measurements system, and outflow measurements system.

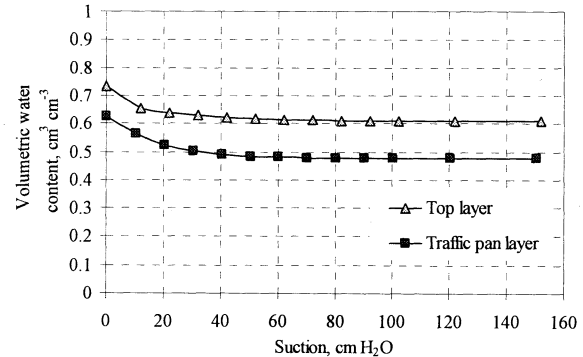


Fig.3 Soil water retention curves of the volcanic ash soils used in the model slope experiments.

4. 2. 1 Soil Packing

The box of $100 \text{ cm} \times 5 \text{ cm} \times 22 \text{ cm}$ for the soil packing of $100 \text{ cm} \times 5 \text{ cm} \times 20 \text{ cm}$ was used for the model slope experiments. All boundaries of the box were impermeable except for the slope surface boundary. The box angle was adjustable about a pivot point located at the outflow end. A screw jack was used to lift the upslope end of the box to vary the slope.

Field soils sieved to pass 2 mm screen were packed into the box at a 60~65% (mass basis) water content. Packing was conducted by hand in a systematic manner to achieve a uniform bulk density for the top (15 cm) and traffic pan (5 cm) layers along the entire length of the model slope.

Traffic pan and top layers were packed in the three and nine incremental stages with the soils, respectively. For packing purposes, the soil was first uniformly spread over the box bed or the surface of the successive layers. Packing was followed by tamping with wooden block and rammer, and then by scraping the surface to maintain a uniform thickness with the sequential layers at the incremental stages.

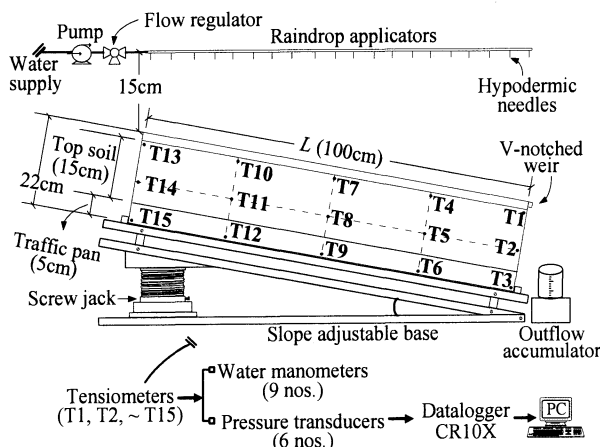


Fig.4 Illustration of the laboratory setup for the model slope experiments.

4. 2. 2 Rainfall Simulator

Raindrops were applied using a drip-type rainfall simulator to cover the slope surface area of $100 \text{ cm} \times 5 \text{ cm}$. The components of the rainfall simulator were: (i) two raindrop applicator pipes arranged in parallel rows and situated along the length of the box; (ii) a set of twenty downward-oriented hypodermic needles (0.6mm inner diameter) accomplished with each applicator pipe along the length; (iii) flow control system; and (iv) constant-discharge pumping system and water supply tubing. Two raindrop applicator pipes delivered a steady rainfall through the set of forty hypodermic needles. The pumping system provided a stable pressure to avoid variations in the rainfall rate during the simulated rainfall event. Different steady rainfall rates were maintained through the flow control system. The outflow from the rainfall simulator and the uniformity of drop pattern were calibrated with the flow control system to achieve the rainfalls similar to those of natural storms of the corresponding rate. In an attempt to prevent erosive impact of the raindrops and to distribute the applied raindrops over the surface, a single layer of gauze was placed on the top of the soil surface. Since applied rainfall rates ($80, 100, 125$, and 150 mm h^{-1}) were restricted to less than the saturated hydraulic conductivity of the top layer, ponding would not occur in the slope surface. Runoff began once the saturated zone intersected the slope surface.

4. 2. 3 Soil Water Pressure Measurements System

Soil water pressure was measured with tensiometers.

The box had fifteen holes on one side in which tensiometers were placed. Tensiometers were placed in such manner that rectangular grids (as in Fig.4, observation nodes T1, T2, T4, and T5 represent a grid, and so forth) were formed.

4. 2. 4 Outflow Measurements System

The box was fitted with a 60° V-notched weir to the point of flow measurement at the outflow end, and water accumulator was provided to collect water flowing over the outflow end. Outflow was manually weighed, and outflow rates were computed using the weight-time method. Suspended soils in the collected outflow waters were settled, dried, and weighed to take into account. Besides, outflow rates were also computed using the volume-time method in order to ensure the reliability of the weight-time computations.

4. 3 Experimental Run

Eight experimental runs were performed, and the experimental runs were designated as 1, 2, 3, 4, 5, 6, 7, and 8 in the order given (Table 1). Each experimental run was carried out until steady state condition of the outflow prevailed. The outflows were observed at 30 minutes interval. Steady state condition for an applied steady rainfall rate was observed by noting the elapsed time when the outflow from the model slope equaled to the influx of rain.

Soil water pressure in the model slope was observed continuously at 30 minutes interval. Soil water pressures of grids were used to define the saturated and unsaturated flow zones. Linear interpolation within each grid was performed to incorporate both the distance and the degree of variation between the known soil water pressure nodes to estimate the values in unknown points under considerations (Cressie, 1991). The positions of the PWT in the model slope and RFGP were assessed from the soil water pressure profiles. The unsaturated zone was defined by the depth from the slope surface to the PWT. The saturated zone was defined by the depth of the PWT. The unsaturated flux at any point under consideration within the each grid was estimated using the Eqs. from (2) to (6). Lateral subsurface flux was estimated by the Eq. (7), and was allowed to occur within the saturated zone.

Table 1 Model slope experimental runs performed in the laboratory

Run designation (No.)	Model slope ($^\circ$)	Rainfall (mm h^{-1})
1	8	80
2	8	100
3	8	125
4	8	150
5	12	80
6	12	100
7	12	125
8	12	150

RFGP was visually inspected to identify the location on the slope surface at which soil loss was considered most likely to initiate, and was followed up to the outflow end.

For each experimental run, RFGP causing water to seep out of the soil followed by caving-in on the slope surface was first visually inspected. The distance of its occurrence was then measured from the upslope to justify the observed RFGP obtained from the matric potential profiles. Bulk densities of the soils in the model slope were gravimetrically determined at a number of locations after each of the experimental run was completed.

5. EXPERIMENTAL RESULTS

Although results of the eight experimental runs have been obtained, it is appropriate to first provide a demonstrative description of the flow field conditions for the experimental run 1. **Fig.5** and **Fig.6** will be referred to in this qualitative description.

5. 1 Evolution of Matric Potentials and the PWT

Matric potential profile of the experimental run 1 is shown in **Fig.5**, indicating that the PWT above traffic pan rises in turn to an increasing depth of saturation downslope and eventually intersects the surface as RFGP. At the PWT matric potential values possess atmospheric. The initial condition is given in **Fig.5a**. At $t = 210$ minutes (**Fig.5b**), negative pressures at the upslope and positive pressures at the downslope regions are observed above traffic pan. The PWT appears above traffic pan at $t = 210$ minutes. The PWT begins to extend up the soil profile at $t = 420$ minutes (**Fig.5c**). On the contrary, traffic pan layer shows negative pressures both at $t = 210$ and $t = 420$ minutes. Steady state condition is attained at $t = 750$ minutes (**Fig.5d**). Nearly the entire flow region is saturated and the PWT intersects the surface. Even at steady state, matric potential patterns indicate the infiltration zone at the upper end of the upslope. Traffic pan eventually undergoes positive pressures, being caused by the weight of the column of the PWT above this layer during the prolonged rainfall.

5. 2 Flux Distributions

Corresponding to **Fig.5**, flux distributions of the representing experimental run 1 is illustrated in **Fig.6**. At $t = 210$ minutes (**Fig.6a**), the infiltrating water is split into two regions with one region at the unsaturated upslope indicating nearly vertical flow, and the other a small saturated region at the downslope above traffic pan indicating both nearly vertical flow at the upper portions and lateral subsurface flow at the saturated zone. At $t = 420$ minutes (**Fig.6b**), the flow in the upper end of the upslope is still nearly vertical, but is being directed into the saturated downslope. Maximum flux appears in the midslope. Flux distributions indicate that saturated conditions extend up only so far as it necessary to accommodate fluxes from the upslope.

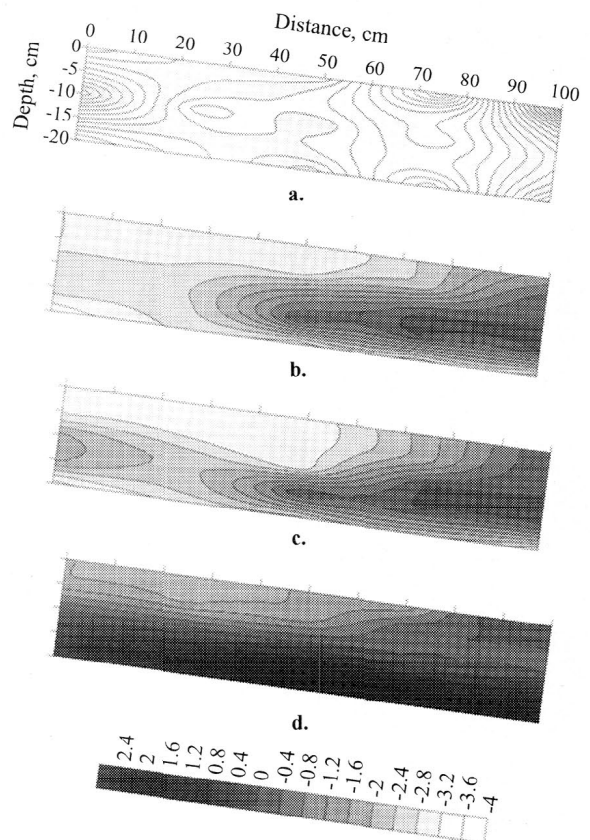


Fig.5 Illustrations of matric potential profile in cm for the 8° model slope experimental run 1 under 80 mm h^{-1} rainfall: (a) initial condition at $t = 0$; (b) at $t = 210$ minutes; (c) at $t = 420$ minutes; and (d) steady state at $t = 750$ minutes. Here, negative sign of labels along the z axis (depth) indicates depth from the surface, and labels used along the x axis (distance) and the z axis (depth) are identical for all the potential profile illustrations hereafter.

However, at this time, there is still tendency for saturated wedge to move up the soil profile and feed the unsaturated zone at the upper end. At steady state (**Fig.6c**), a large region of the flow is parallel to the slope in the midslope and downslope regions, and a possible small region of return flow is over the downslope end at RFGP. Maximum flux is observed at RFGP section. Observation of the unsaturated zone at the upper end of the upslope (as shown in **Fig.5d**) suggests that this unsaturated portion allows the further rainwater entry in the model slope even at steady state.

Matric potential profiles and flux distributions at steady state for the experimental runs 2, 3, and 4 of the 8° , and runs 5, 6, 7, and 8 of the 12° model slope experiments are illustrated in **Fig.7** and **Fig.8**, and **Fig.9** and **Fig.10**, respectively. Trends of the flow processes for these runs are similar to that described in the experimental run 1.

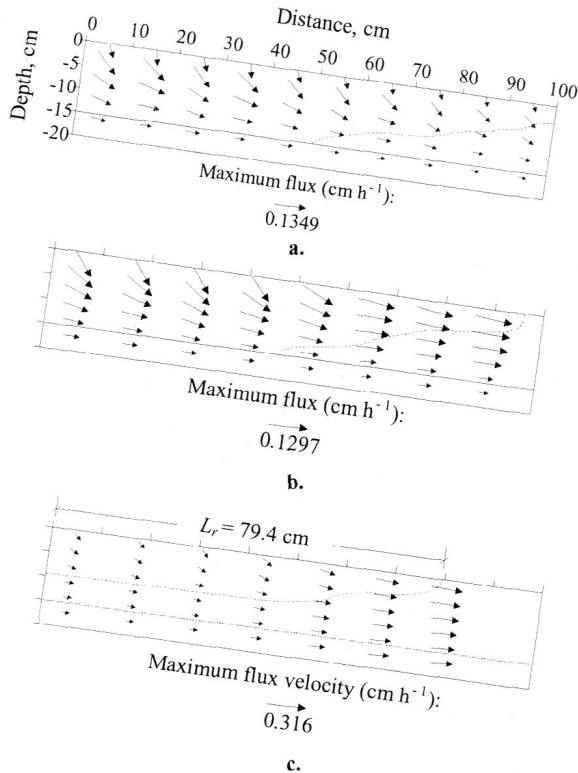


Fig.6 Illustrations of flux distributions in cm h^{-1} for the 8° model slope experimental run 1 under 80 mm h^{-1} rainfall: (a) at $t = 210$ minutes; (b) at $t = 420$ minutes; and (c) steady state at $t = 750$ minutes, RFGP occurs at 79.4 cm from the upslope. Corresponding to matric potential profiles, dashed lines represent the positions of the PWT. Labels used along the x axis (distance) and the z axis (depth) are identical for all the flux distribution illustrations hereafter.

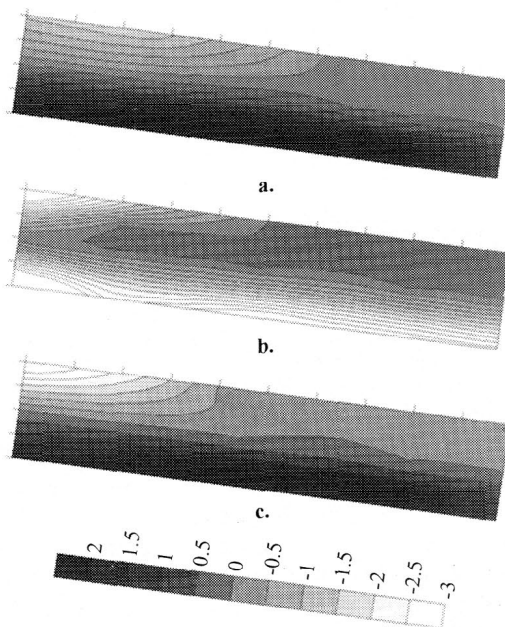


Fig.7 Illustrations of matric potential profiles in cm for the 8° model slope at steady state: (a) experimental run 2 applying 100 mm h^{-1} rainfall, $t = 720$ minutes; (b) run 3 applying 125 mm h^{-1} , $t = 600$ minutes; and (c) run 4 applying 150 mm h^{-1} , $t = 630$ minutes.

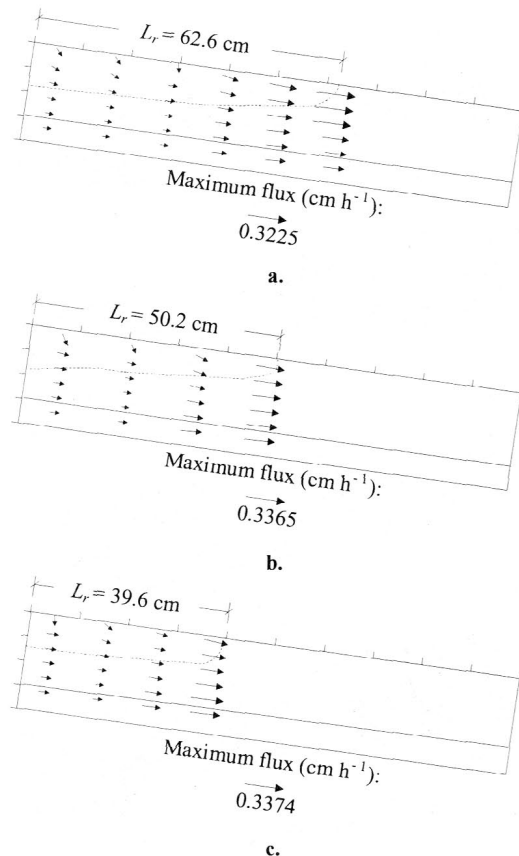


Fig.8 Illustrations of flux distributions in cm h^{-1} for the 8° model slope at steady state: (a) experimental run 2 applying 100 mm h^{-1} rainfall, $t = 720$ minutes; (b) run 3 applying 125 mm h^{-1} , $t = 600$ minutes; and (c) run 4 applying 150 mm h^{-1} , $t = 630$ minutes. Dashed lines represent the positions of the PWT and thus RFGPs.

However, negative pressures within traffic pan only for the run 3 (Fig.7b) suggest that this run might have been prolonged to achieve complete steady state than that of the existing pseudo-steady state during the experimentation. At least in Fig.8b, flow for run 3 did not reach steady state. The outflow hydrograph, as shown in Fig.14, confirms that steady state condition for the experimental run 3 has been attained. Conceptually, traffic pan undergoes positive pressures at steady state caused by the weight of the overlying column of the PWT, and by the slow penetration of the wetting front into it during the prolonged rainfall. The unsaturated traffic pan soils apparently clarified that steady state was not completely achieved for this experimental run.

5. 3 Observed RFGP

Observed RFGPs for the 8° and 12° model slope experimental runs are summarized in Table 2. The visual inspections of RFGPs, as also shown in Table 2, justify the observed RFGPs obtained from the matric potential profiles.

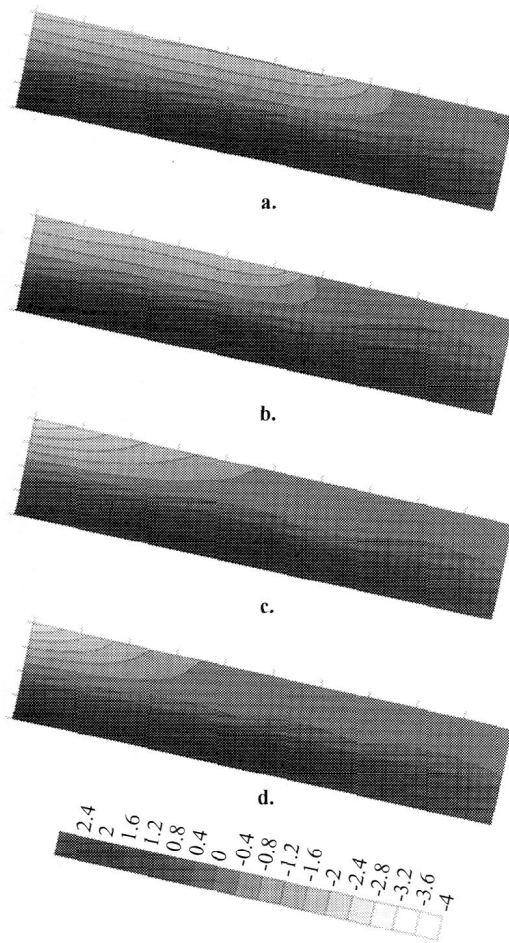


Fig.9 Illustrations of matric potential profiles in cm for the 12° model slope at steady state: (a) experimental run 5 applying 80 mm h⁻¹ rainfall, $t = 720$ minutes; (b) run 6 applying 100 mm h⁻¹, $t = 700$ minutes; and (c) run 7 applying 125 mm h⁻¹, $t = 630$ minutes; and (d) run 8 applying 150 mm h⁻¹, $t = 600$ minutes.

As mentioned before, visual inspections were performed to identify the breakout location of the PWT on the slope surface at which erosion was likely to initiate, and followed up to the outflow end of the box. For a demonstrative purpose, **Fig.11** depicts that RFGP is visualized on the slope surface at 80 cm distance from the upslope, and erosion also initiates at 80 cm for the experimental run 1.

6. DISCUSSION

6. 1 Flow Produced by Traffic Pan

Each of the model slope experimental runs, conceptualized for Tsumagoi hillslope in **Fig.2**, extends the norm of the generalized saturated subsurface flow produced by traffic pan. Build-up of the saturated zone is triggered with the hydraulic conductivity contrast between the top and traffic pan layers.

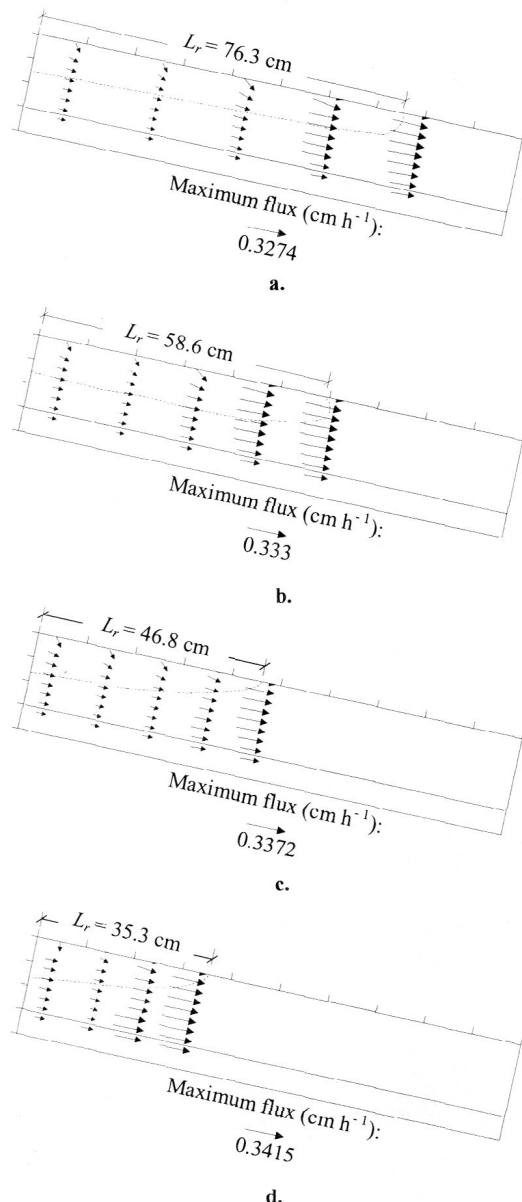


Fig.10 Illustrations of flux distributions in cm h⁻¹ for the 12° model slope at steady state: (a) experimental run 5 applying 80 mm h⁻¹ rainfall, $t = 720$ minutes; (b) run 6 applying 100 mm h⁻¹, $t = 700$ minutes; and (c) run 7 applying 125 mm h⁻¹, $t = 630$ minutes; and (d) run 8 applying 150 mm h⁻¹, $t = 600$ minutes. Dashed lines show the positions of the PWT and thus RFGPs.

Traffic pan restricts the downward movement of soil water significantly, and causes soil water pressures to rise. Consequently, traffic pan causes the perching of soil water as the PWT, leading to saturated subsurface flow. Such PWT is obviously disconnected from the regional groundwater table, and is dependent on the nature and spatial distribution of existent traffic pan, as well as on the depth of top layer.

6. 2 Implications of RFGP Approach

RFGP derived for the response of hillslope layered with existent traffic pan addresses the slope saturation under steady state condition. The temporal changes in RFGP owing to the inherent saturated areas at the bottom of the hillslope have not been considered.

Table 2 RFGPs observed in the 8° and 12° model slope experiments

Run	Model slope (°)	Rainfall (mm h ⁻¹)	Observed RFGP, L_r (cm)	
			Visual inspection	Matric potential profile
1	8	80	80	79.4
2	8	100	62	62.6
3	8	125	50	50.2
4	8	150	40	39.6
5	12	80	76	76.3
6	12	100	59	58.6
7	12	125	47	46.8
8	12	150	35	35.3

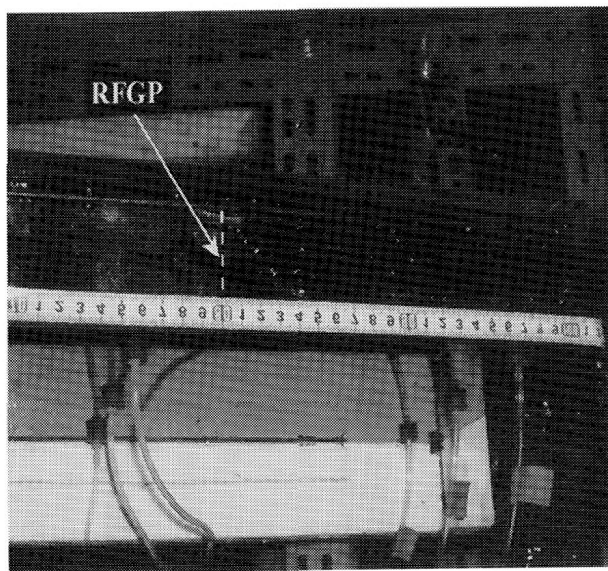


Fig.11 Visual inspection of RFGP on the downslope surface for the 8° model slope experimental run 1 under 80 mm h⁻¹ rainfall at steady state. Picture shows the top view of the downslope. RFGP is measured at 80 cm (dashed line across the slope surface) from the upslope. Erosion is most likely to start at 80 cm and is followed up to the outflow end, indicating the occurrence of RFGP at 80 cm from the upslope.

6. 2. 1 The Observed versus Predicted RFGP

It is more likely that all the terms in the Eq. (9) have the same proportional effect on RFGP (L_r) at steady state. Since K_s , A , and α are known parameters L_r could also be predicted. Subsequently, a qualitative comparison between the observed (L_r) and the predicted (L_{rc}) is demonstratively made for the 8° model slope experiments under the applied four rainfalls (Fig.12). The predicted RFGPs are somewhat erratic within the variability of the observed RFGPs. The observed RFGPs are relatively higher than predicted values, i.e., the observed RFGPs provide less slope saturation.

The reason might be attributed to the relatively less inclination of the PWT observed in the model slope experimental runs. Although the Eq. (9) for predicting RFGP assumes that the inclination of the PWT is equal to the slope surface, the inclination of the PWT was always observed less than the surface slope. The PWT was inclined concave downward towards the upslope from the intersection of the PWT and the slope surface throughout the experimental run. Such position of the PWT in the model slope increased only the downslope saturated depth as well as discharge through the saturated slope surface (Weyman, 1973), but the advance of the PWT towards the upslope surface was rather slow. Consequently, the observed RFGPs were relatively higher than those predicted theoretically, indicating less slope surface saturation.

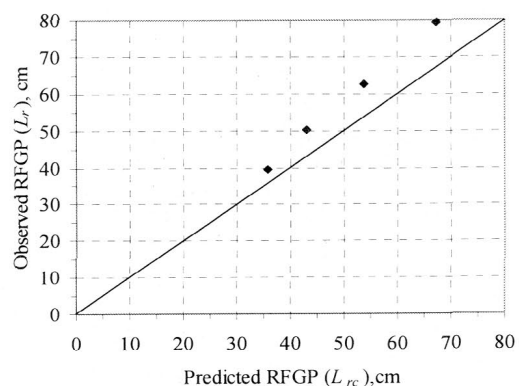


Fig.12 The Observed RFGP versus the predicted RFGP for the 8° model slope experimental runs 1, 2, 3, and 4 under the steady rainfalls of 80, 100, 125, and 150 mm h⁻¹, respectively. The 1 to 1 relationship is represented by the solid line.

6. 2. 2 Rainfall Rates and Slope Angles on RFGP

The effect of the rainfall rates on RFGP is a direct one, since the rate of growth of the PWT depends strongly on the rainfall rates. Table 2 shows that the rainfall rate is inversely related with RFGP. RFGPs decrease because of high rainfall rates, indicating more slope surface saturation. However, the increment varies for the different rainfalls such that this incremental variation does not emphasize any certain extent, suggesting the significant nonlinearities in the occurrence of RFGP with respect to the rainfall rates. Since each of the experimental runs approached downslope subsurface flux ensues at steady state, RFGP could be represented demonstratively as function of the rainfall rates (r) based on the experimental runs 1, 2, 3, and 4 by using the Eq. (8). Subsequently, prediction for RFGPs (L_{rc}) could be extended theoretically to a range of the rainfall rates. Fig.13 shows r as a function of L_{rc} .

Surface runoff routing was not needed to study this model hillslope, since saturation was always proceed upward from the below. This condition was insured by the fact that the rainfall rates applied were much lower than the saturated hydraulic conductivity of the top soil.

Runoff began once the saturation intersected the slope surface. Therefore, the mechanism that produced runoff was saturation overland flow. The outflow hydrographs, demonstratively shown in Fig.14, show the saturation overland flows for the 8° model slope experimental runs 1, 2, 3, and 4 under the steady rainfalls of 80, 100, 125, and 150 mm h⁻¹, respectively.

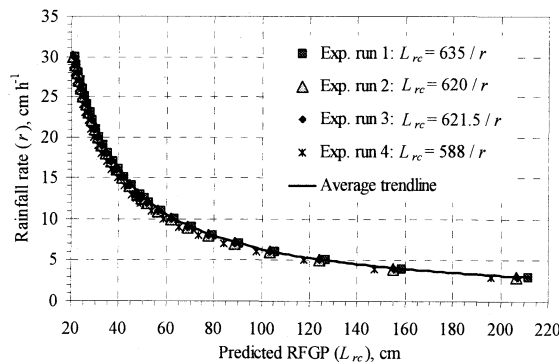


Fig.13 The predicted RFGP as the function of the different steady rainfalls derived from the 8° model slope experimental runs 1, 2, 3, and 4 under the steady rainfalls of 80, 100, 125, and 150 mm h⁻¹, respectively, and extended to a range of the rainfall rates.

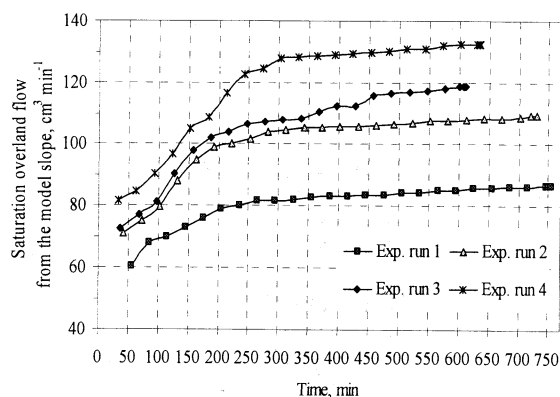


Fig.14 Saturation overland flow (return flow coupled with the direct rainfall onto the saturated areas) for the 8° model slope experimental runs 1, 2, 3, and 4 under the steady rainfalls of 80, 100, 125, and 150 mm h⁻¹, respectively.

As shown in Table 2, RFGPs slightly decrease due to increase in the slope angles from 8° to 12°, indicating that the 12° model slope experimental runs slightly increase surface saturation. In the Eq. (9), this is not the case. The slope saturation is likely to be increased due to increase in the slope angles. The PWT expands more and tapers off in the upslope direction, advancing RFGPs to be occurred at the relatively upper locations for the 12° experimental runs than RFGPs for the 8° experimental runs. This may be explained by considering the development of the rising PWT in the model slope. The prolonged rainfalls create a corresponding increase in the saturated thickness, and thereby extending the PWT up the soil profiles.

For small slope angles, the available storage profile in the hillslope is theoretically a thin, triangular saturated wedge over most of the slope length. In the relatively steep slopes, the available storage profile is more rectangular in shape for the expansion of the PWT. However, since very gentle slopes (8° and 12°) were chosen in this study, it is suggested that more observations may be necessary for the steep slopes (i.e., usually 20~30° for hillslope fields) to clearly recognize the effect of the slope angles on RFGP.

6. 2. 3 Slope Length on RFGP

RFGP is the PWT intersection dependent attribute on a uniform hillslope surface. In all the experimental runs, RFGPs were observed such that $L_r \leq L$ (Table 2). However, referred to Fig.2, slope length L (100 cm in this study) does not experience RFGP unless the PWT intersects the surface. RFGP at steady state, predicted by the Eq. (9), has also been derived based on the location of the intersection of the PWT and the slope topography. Although a long slope increases the available storage profile, RFGP defined in this study generally does not depend on the slope length. RFGP must be observed on the long hillslope wherever the PWT intersects the slope surface during the prolonged rainfall episodes.

6. 2. 4 Erosion Process at RFGP

RFGP is more likely to commence at the location where gullies and rills are often formed. Qualitatively, RFGP may explain such field erosion phenomena on the acceptance of two processes: (i) outcoming water erodes the soil right at RFGP, and (ii) water comes out of the soil as return flow and contributes to surface runoff. The first interpretation is undoubtedly outward seepage of water that, by itself, may be an erosive mechanism. The seepage forces imposed on the soil particles by the drag of outflowing water between the particles can detach the soil particles (Gabbard et al., 1998). This upward-directed seepage force is inconceivable without water coming out of the soil. When it does at RFGP, it possesses so at positive pressures, while at the same time the slope surface is nearly saturated. The second interpretation is that saturation overland flow is initiated at RFGP. Since subsurface flow through the saturated zone encounters a seepage face at the slope surface, subsurface flow process may grade into return flow by which subsurface water contributes to surface runoff, and obviously accelerates gullies and rills.

7. CONCLUSIONS

The following conclusions are drawn on the basis of model slope experiments performed in this study:

- 1) Traffic pan causes hillslope saturation because of the rising PWT fed by infiltration into the unsaturated zone and by laterally inflowing subsurface flow through the saturated zone during the prolonged rainfalls.

- 2) Prediction for the occurrence of the surface saturation on a uniform hillslope layered with traffic pan under steady state is approached as RFGP, which is referred to as the location of the intersection of the PWT and the slope surface attributed to the return of infiltrated rainwater. Erosion is most likely to initiate at RFGP on the hillslope topography.
- 3) RFGP observed in the model slope experiments is in essential agreement with the predicted RFGP under the different steady rainfalls.
- 4) Rainfall rates are inversely related with RFGP. RFGP decreases because of high rainfall rate, i.e., increase in hillslope saturation. Although a small increase in the slope angles results the decrease in RFGP, it is suggested that observations may be necessary for the steep slope angles to recognize the effect.
- 5) For a long uniform hillslope, it is envisaged that RFGP defined in this study must be observed wherever the PWT intersects the hillslope topography during the prolonged rainfalls.

ACKNOWLEDGEMENTS : The authors wish to express gratitude to Mr. Imoto Hiromi, the University of Tokyo, for his technical assistance during the laboratory experiments. Gratitude is also expressed to Mr. Hinoto Masatoshi, Alpine Crops Research Center, Tsumagoi, Gunma Prefecture, for his assistance during the field investigations. Thanks are extended to Mr. Hamamoto Shoichiro, the University of Tokyo, for his help in editing the manuscript. In addition, the authors wish to express gratitude to the two anonymous reviewers for their comments that helped to strengthen the manuscript.

REFERENCES

- Aryal, S. K., O'Loughlin, E. M., and Mein, R. G. (2002): A similarity approach to predict landscape saturation in catchments, *Water Resour. Res.*, Vol.38, 26/1-14.

- Anderson, M. G., and Burt, T. P. (1990): Subsurface runoff, In: Anderson, M. G., and Burt, T. P. (eds.), *Process studies in hillslope hydrology*, John Wiley and Sons, Chichester, 365-400.
- Cressie, N. A. C. (1991): *Statistics for spatial data*, John Wiley and Sons, New York, p.900.
- Dunne, T., Moore, T. R., and Taylor, C. H. (1975): Recognition and prediction of runoff producing zones in humid regions, *Hydrolog. Sci. Bull.*, Vol.20, 305-327.
- Gabbard, D. S., Huang, C., Norton, L. D., and Steinhardt, G. C. (1998): Landscape position, surface hydraulic gradients, and erosion process, *Earth Surf. Processes Landforms*, Vol.23, 83-93.
- Huggett, R. S. (1975): Soil landscape systems: A model of soil genesis, *Geoderma*, Vol.13, 1-22.
- Miyazaki, T. (1993): *Water flow in soils*, Marcel Dekker, New York, p.296.
- O'Loughlin, E. M. (1981): Saturation regions in catchments and their relations to soil and topographic properties, *J. Hydrol.*, Vol.53, 229-246.
- van Genuchten, M. Th., Leij, F. J., and Yates, S. R. (1991): The RETC code quantifying the hydraulic functions of unsaturated soils, *Rep. No. EPA/600/2-91/065, U.S. Salinity Laboratory, USDA, ARS, Riverside, CA*, p.85.
- Wallach, R., and Zaslavsky, D. (1991): Lateral flow in a layered profile of an infinite uniform slope, *Water Resour. Res.*, Vol.27, 1809-1818.
- Whipkey, R. Z., and Kirkby, M. J. (1978): Flow within the soil, In: Kirkby, M. J. (ed.), *Hillslope hydrology*, John Wiley and Sons, Chichester, 121-144.
- Weyman, D. R. (1973): Measurements of the downslope flow of water in a soil, *J. Hydrol.*, Vol.20, 267-288.
- Zaslavsky, D., and Sinai, G. (1981a): Surface hydrology: I - Explanation of phenomena, *J. Hydraulics Div., ASCE*, Vol.107 (HY1), 1-16.
- Zaslavsky, D., and Sinai, G. (1981b): Surface hydrology: III - Causes of lateral flow, *J. Hydraulics Div., ASCE*, Vol.107 (HY1), 37-52.

[Received 2005. 2. 14, Accepted 2006. 1. 10]

[Questions and/or discussions on this paper for public debate will be accepted before 2006. 8. 24]

耕盤層を有する成層斜面中の復帰流発現点

DEB Sanjit Kumar

宮崎 育

溝口 勝

関 勝寿

東京大学大学院農学生命科学研究科, 〒113-8657 東京都文京区弥生1-1-1.

要旨

モデル斜面を用いて、耕盤層を有する不飽和成層斜面中における降雨浸潤下での二次元の水分移動を明らかにした。モデル斜面（斜度 8°、12°）に異なる定常降雨強度（80, 100, 125, 150 mm h⁻¹）を与えると、斜面方向への側方流の発生だけでなく耕盤層上方において宙水的な地下水面（Perched Water Table、PWT）が発達した。定常状態における飽和域で発生する流れに注目し、斜面における表面飽和の形成を予測する概念として、復帰流発現点（Return Flow Generating Point、RFGP、降雨浸潤により復帰した斜面中の宙水的な地下水面が地表面と交差する点）を導入した。8回の実験から観測された RFGP について考察し、耕盤層の有する均一な成層長斜面における RFGP の意味を明らかにした。

キーワード：不飽和土壌、耕盤層、モデル斜面、復帰流発現点